Expansion of a Holepunch Cloud by a Gravity Wave Front

DAVID J. MURAKI

Department of Mathematics, Simon Fraser University, Burnaby, British Columbia, Canada

RICHARD ROTUNNO AND HUGH MORRISON

National Center for Atmospheric Research, Boulder, Colorado*

(Manuscript received 24 July 2015, in final form 21 October 2015)

ABSTRACT

A holepunch cloud is a curious phenomenon where a disturbance in a thin cloud layer initiates an expanding circular hole of clear air. Usually triggered by the passage of aircraft, observations of these holes in clouds date back to the earliest days of aviation, but only recently has a holepunch cloud been simulated within a full-physics numerical model. These computations confirm that ice crystal growth through the Wegener–Bergeron–Findeisen process creates a small cloud-free region whose subsequent outward spread defines the holepunch. The mechanics behind this continued expansion, however, has yet to be definitively identified. In this article, the motion of the cloud edge is explained as a propagating gravity wave front. To support this idea, a hierarchy of three idealizations is analyzed: a full-physics numerical model, a fluid mechanical model with simplified moisture effects, and a conservation law analysis for front motion. The essence of the holepunch cloud is established to be a moist air layer that is unsaturated (clear) and weakly stratified within the hole but saturated (cloudy) and moist neutral outside of it. The cloud edge thus represents a barrier to the outward propagation of gravity waves within the clear air—the result of this collision is a wave front whose velocity determines the growth rate of the hole.

1. Introduction

A holepunch cloud is the picture-worthy phenomenon of a near-circular patch of clear air puncturing a thin supercooled cloud layer (Schumacher 1940). It is usually accompanied by a fallstreak of ice crystals associated with the center of the clearing, so it is sometimes called a fallstreak hole. Most often initiated by the penetration of a cloud layer by either ascending or descending aircraft, these holes can grow to several kilometers in radius over time periods exceeding an hour. A linear version, called a canal cloud (Fig. 1), can also result from a level flight track within a cloud layer (Poulter 1948; Simon 1966). Long an atmospheric fascination for scientists (Hobbs 1985; Pedgley 2008) and weather enthusiasts alike [eliciting editorial responses from Ludlam (1956) and Scorer (1964)], recent advances have provided new quantitative insights into the holepunch phenomenon. In 2010, two instrumented observations of holepunch cloud events were reported (Westbrook and Davies 2010; Heymsfield et al. 2010) that reveal structural details, such as lidar retrievals of vertical velocities and liquid water content. Subsequently, a full-microphysics simulation based upon these observations has since shown that ice crystal growth can initiate both the dissipation of cloud and the flow dynamics leading to the subsequent expansion of a circular hole (Heymsfield et al. 2011). This article presents a fluid mechanical explanation for the growth of the hole within the cloud layer. In particular, we identify the ''wave perturbation propagating outward from a central initiation area,'' as observed by Johnson and Holle (1969), to be a gravity wave whose leading-edge front of downward motion evaporates the cloud and enlarges the hole.

a. Evolution of the holepunch

The numerical simulation of Heymsfield et al. (2011) provides a clear narrative for the holepunch cloud

* The National Center for Atmospheric Research is sponsored by the National Science Foundation.

Corresponding author address: David J. Muraki, Department of Mathematics, Simon Fraser University, 8888 University Drive, Burnaby BC V5A 1S6, Canada.
E-mail: muraki@math.sfu.ca

DOI: 10.1175/JAS-D-15-0211.1

FIG. 1. Photo of a canal cloud segment. The slight curvature is a distortion due to the panoramic perspective. (Photo credit: Liem Bahneman, 2010).

development (observed values upon which this case is based are shown in parentheses). The background environment is a thin (150 m) supercooled cloud layer (−30°C at 7.8-km altitude) bounded above and below by stable, dry air. The dynamics are initiated by a localized (250-m wide) introduction of ice crystal particles throughout the depth of the moist layer. The microphysical response begins with rapid depletion of the liquid cloud by the Wegener–Bergeron–Findeisen (WBF) process, with a net release of the latent heat of fusion, and continuation of ice growth by vapor deposition, with its latent heat of sublimation. The latent heating results in upward motion with compensating downdrafts peripheral to the central ice particle region. As simulated in (Heymsfield et al. 2011), these downdrafts accelerate evaporation of liquid water, and the hole rapidly widens over time (4.4-km diameter after 90 min). While the simulation was clear on this sequencing of events for the formation of the hole, a definitive causal mechanism for the sustained expansion of the hole was not identified. Specifically, factors that determine the speed of the cloud edge remained unaddressed.

Candidate explanations for the growth of the holes are discussed in both Pedgley (2008), Heymsfield et al. (2010), as well as in follow-up comments to the latter (Hindman 2013; Heymsfield 2013). The first category of these involves WBF activity at the cloud edge, where the radial dispersion of ice particles could be driven by turbulent diffusion, weak convection, or wake turbulence. The second category is related to a global circulation (on the scale of the hole) whereby continuous latent heating within clear air (by WBF vapor deposition) strengthens the central updraft, thus inducing subsidence with an increasing outward extent. Both lines of thought require persistent ice microphysical activity, either local to the cloud edge, or at the core. In this article, we present the distinct mechanism of a free-propagating gravity wave that requires no direct microphysical forcing to sustain its motion.

b. An explanation for the growth of the holepunch

Our theory for the holepunch growth begins by understanding the particular idealization to a marginal cloud layer whose liquid water content is sufficiently low that its dissipation can be captured by small displacement, linear dynamics. Only a two-dimensional cross-sectional version of the holepunch is considered—this corresponds to the canal cloud geometry (Fig. 1). The theory is developed through a sequence of three idealizations for the holepunch dynamics: a full-microphysics simulation of an artificially weak cloud layer, a two-dimensional fluid model with a buoyancy response that switches for saturated and unsaturated moist air, and a further reduced one-dimensional analysis for the outward propagation speed of the cloud edge.

The presentation starts with a summary of the background environment for a control run showing the holepunch dynamics. It is demonstrated that, within simulations that reproduce the holepunch, the WBF and ice processes that initiate the hole are not the primary driver for its continued expansion. Then, it is shown that the behavior of the holepunch cloud is essentially unaffected by a weakening of the liquid water content of the cloud. From these simulations, we identify the key gravity wave feature to be a warm anomaly within the clear air that is propagated by vertical motions that warm on the outward side and cool on the inward side. The downward motion on the leading edge also evaporates cloud water and expands the hole. These results motivate the development of a two-dimension fluid dynamical model that simplifies the moisture physics: cloudy air is moist neutral, and clear air is weakly, but stably, stratified. For initial conditions and latent heat forcing consistent with the WBF process, this fluid model reproduces a gravity wave front whose cloud-edge dynamics compares well against the full-microphysics simulation. The frontal nature of the wave is a consequence of the fact that cloudy air that is moist neutral does not permit a buoyancy response that supports gravity waves—thus the cloud edge represents an

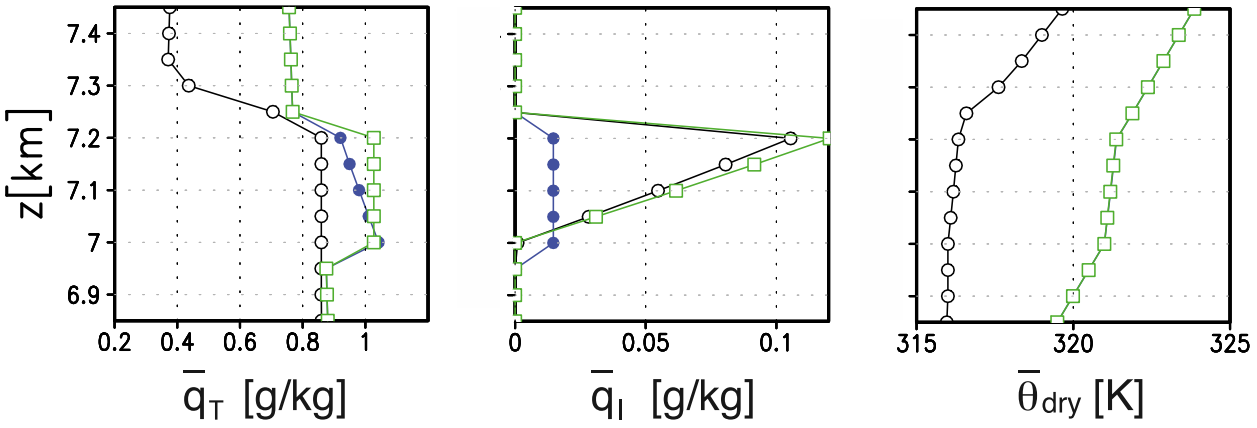

FIG. 2. Initial thermodynamic profiles ($\overline{q}_T$, $\overline{\theta}_{dry}$) with CTL shown in black, ADC in green, and UNC in blue (Table A1). The 250-m adiabatic moist neutral layer resides in the height range $7.00 < z < 7.25$ km, but the UNC layer is shifted downward 25 m. Within this layer, the CTL and ADC profiles have constant total water mixing ratio $\overline{q}_T$, which also implies moist adiabatic or constant moist entropy $\overline{\theta}_e$. The UNC profile has uniform liquid cloud water mixing ratio $\overline{q}_l$, and total cloud liquid reduced to one-quarter of ADC. The $\overline{\theta}_{dry}$ plot illustrates the adjustment for increased stability below the moist layer used for the idealized runs (ADC and UNC). The LIM and WAV runs use the CTL profiles.

impediment to propagation. Finally, to address the question of what happens when the outward-propagating wave impinges upon this moist neutral barrier, a type of immersed boundary approximation is applied to reduce the fluid model to a one-dimensional analysis of the gravity wave front speed. It is shown that the cloud-edge velocity satisfies a Rankine–Hugoniot condition that quantifies the slowing of the gravity wave front by the neutrality of the cloudy air.

2. Simulations of holepunch clouds

a. Two-dimensional, full-physics experiments

A baseline for understanding the holepunch dynamics is established through a two-dimensional adaptation of the Weather Research and Forecasting (WRF) Model simulations of Heymsfield et al. (2011). Results from our experiments are described here, with details of the model setup and experimental design deferred to the appendix. The initial thermodynamic profiles (Fig. 2) are based upon sonde observations from the original holepunch simulation, but with a refinement that imposes exact moist neutral and moist adiabatic conditions consistent with the WRF thermodynamics (Miglietta and Rotunno 2005). This consistency was found to be important for limiting convective instability leading to dissipation of the cloud layer. In addition, background wind shear is removed so that the flow pattern is driven solely by the holepunch initiation.

The control (CTL) run (Fig. 3) produces the expected holepunch in a 250-m-deep moist layer whose cross-sectional features evolve analogously to the three-dimensional simulations of Heymsfield et al. (2011). Rapid growth of ice by vapor deposition in the supersaturated environment leads to an immediate loss of liquid cloud water by the WBF mechanism. Continued latent heating drives a warm anomaly in the hole center, which in turn drives upward air motion (Fig. 3a). This sets up a circulation in which compensatory downward motion at the hole edges erodes the cloud, and horizontal spreading of the warm anomaly then leads to its eventual splitting (Fig. 3b). This outward dynamics continues and results in a lateral growth of the hole at a near-constant rate of $0.6 \pm 0.1\,\mathrm{m\,s^{-1}}$ (Fig. 3c). Conversion of cloud ice to snow produces precipitation beneath the hole (not shown, but is like the fallstreak in Fig. 1) that is consistent with previous observations of holepunch clouds (Westbrook and Davies 2010; Heymsfield et al. 2010). Evolutions for longer time (as illustrated by the LIM run in section 5) indicate a weakening of the central updraft that runs counter to an enlarging global circulation as a simple explanation for the growth of the hole. Moreover, the phasing of the warm anomalies with downward motion on the outward side does support the idea of a gravity wave feature driving the cloud-edge motion.

Next, we eliminate the other ice physics-driven hypothesis (direct WBF erosion) for the cloud-edge motion. The second experiment (LIM) is identical to the CTL run in initialization but limits the WBF microphysics to a center zone ($-250 < x < 250$ m, green shaded) containing the region of initially injected ice. Figure 4a shows this LIM run to be virtually identical at 15 min with the CTL evolution (Fig. 3c)—except for slightly weaker warm anomalies. The similarity of the

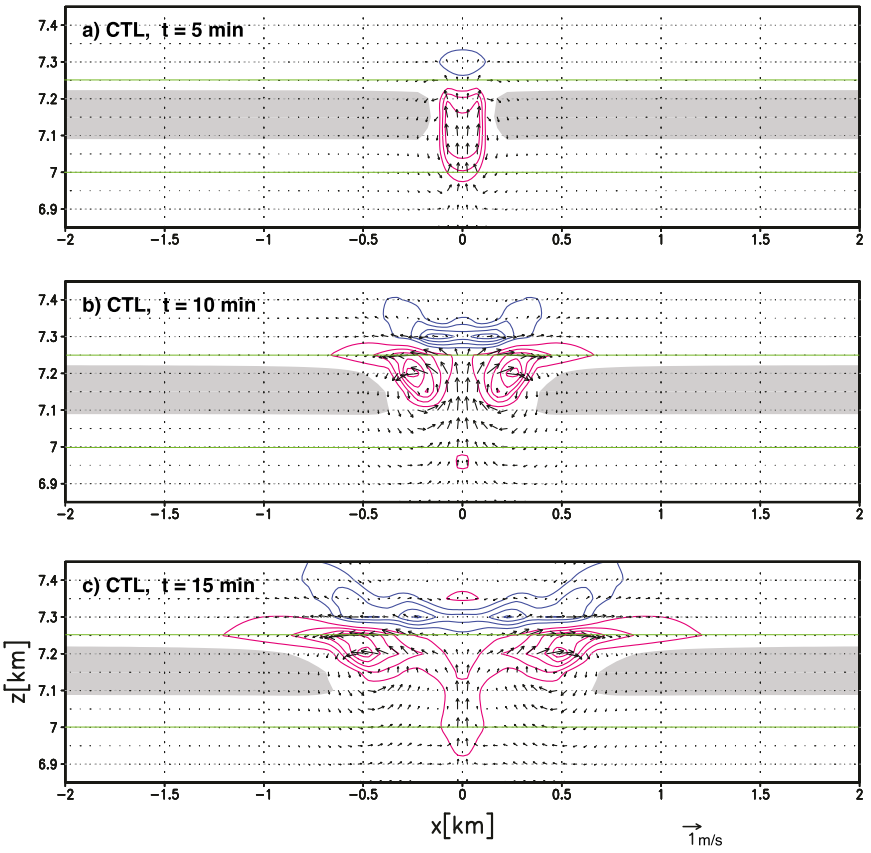

FIG. 3. Control (CTL) simulation of a holepunch in an adiabatic cloud layer. Temperature anomalies are contoured (warm in red, cold in blue) at 0.1-K intervals (zero contour not shown). Velocity is indicated by black arrows, scaled on 1 m s^{-1}. The initial moist-layer region is delineated by thin green lines, and light shading indicates regions of liquid water mixing ratio q_l above 5×10^{-2} g kg^{-1}.

LIM holepunch beyond the WBF zone to the CTL runs clearly demonstrates that the movement of the cloud edge is not a direct result of local microphysics but again implicates a more dynamical explanation.

b. *Idealized experiments*

To investigate the gravity wave hypothesis for the hole growth, we introduce two simulations with more idealized background profiles. Both the adiabatic cloud (ADC) and uniform cloud (UNC) runs involve moist neutral layers embedded within a more symmetric (relatively) dry environment. Specifically, the air immediately above and below the moist layer is given constant static stability ($d\theta_{\rm dry}/dz = 0.01$ K m^{-1}) and a relative humidity of 85% that reduces the effects of entrainment at the cloud top (Fig. 2). As evident in (Fig. 4b), embedding the moist neutral and moist adiabatic cloud layer (ADC) in this more symmetric environment yields an essentially unchanged holepunch, but with gravity waves now apparent in the temperature contours beneath the cloud layer. Found just below the levels of cloud water, these waves appear where ripples in the lidar Doppler vertical velocity were observed by Westbrook and Davies (2010).

However, it is a property of the adiabatic cloud profile that the lifting condensation level for any cloud parcel is the initial cloud bottom. So, clear air appearing within the moist-layer region resulting from resolved-scale vertical motion (rather than microphysics or numerical mixing) must be a (relatively dry) parcel originating from outside the moist layer. The expansion of the holepunch in an ADC layer therefore implies vertical displacements that scale with the moist-layer thickness itself.

This motivates the consideration of an alternative cloud profile: one with uniform liquid water. As discussed in the appendix, such a layer has displacements from the lifting condensation level that are controlled by the amount of liquid water in the cloud [Eq. (A1)].

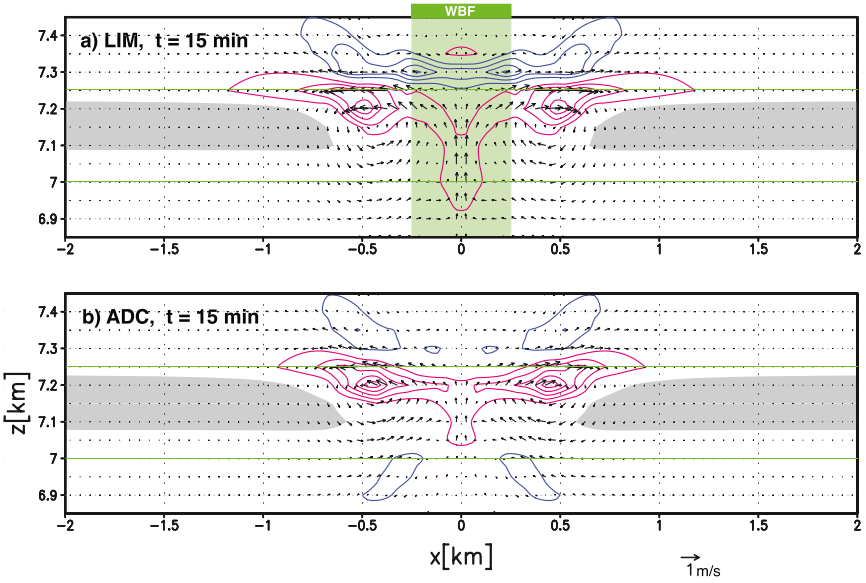

FIG. 4. Comparative simulations of a holepunch after 15 min, with fields as shown in Fig. 3. (a) The LIM run differs from CTL only in that the WBF ice processes is limited to within ±0.25 km from center (green shaded region). (b) The ADC run is modified from CTL mainly in that the environments above and below the moist neutral layer are made more symmetric and idealized. Despite their alteration, both runs show qualitatively similar development with the CTL run.

In addition, this uniform liquid water cloud (UNC) has a moist layer whose vertically integrated liquid water is reduced to one-quarter of the ADC case. We estimate that for most of the UNC initial cloud (Fig. 2), evaporation of all the liquid water in any parcel requires, at most, a downward displacement of roughly 25 m. This is considerably less than the 250-m total depth of the moist layer and, thus, embodies the marginal cloud assumption, whose theory is presented in the next section. The simulated holepunch for the UNC case is shown in Fig. 5 and, despite that the dynamics involved are weaker relative to CTL and ADC (note the differing wind arrow scales), there follows a qualitatively similar narrative for the growth of the hole. The times are chosen to reflect development stages that roughly parallel those of CTL (Fig. 3). Note that the gray shading of the liquid water mixing ratio q_l reflects the uniformity of the UNC cloud, in contrast to the ADC case where the most dense cloud is just below the layer top. The central updraft barely remains after the splitting of the warm anomaly (time $t = 17$ min and beyond).

In all of the simulations, the outward expansion of the cloud edge is trailed by a localized warm anomaly with a circulation whose phase strongly suggests a propagating gravity wave (Cushman-Roisin 1994). However, a question arises regarding the interplay between this gravity wave feature and the moist neutral cloud, where the absence of buoyancy effects precludes wave propagation. This is further investigated through the development of theoretical models presented in the next two sections.

3. Fluid dynamics for a moist neutral layer

As evident from the simulations, the relationship of the holepunch cloud dynamics to the fluid motions is a coupling intermediate to familiar situations of advection of stable clouds and unstable growth of convective clouds. In this section, a simple extension is made to the primitive fluid equations that includes the nonprecipitating dynamics of a moist neutral layer. The model incorporates only one additional feature to account for the moisture effects, a buoyancy switch that is a change of the stratification parameter depending on whether the moist fluid is saturated or unsaturated. The development of such a buoyancy switch follows an early use by Bjerknes (1938), an integration into a cloud dynamics by Kuo (1961), and a thermodynamic derivation by Bretherton (1987). More recently, the switch idea has been revived for understanding clusters of conditionally unstable (and nonprecipitating) clouds (Pauluis and Schumacher 2010, 2011). For an evolving cloud, the key component in the switch formulation is a dynamical

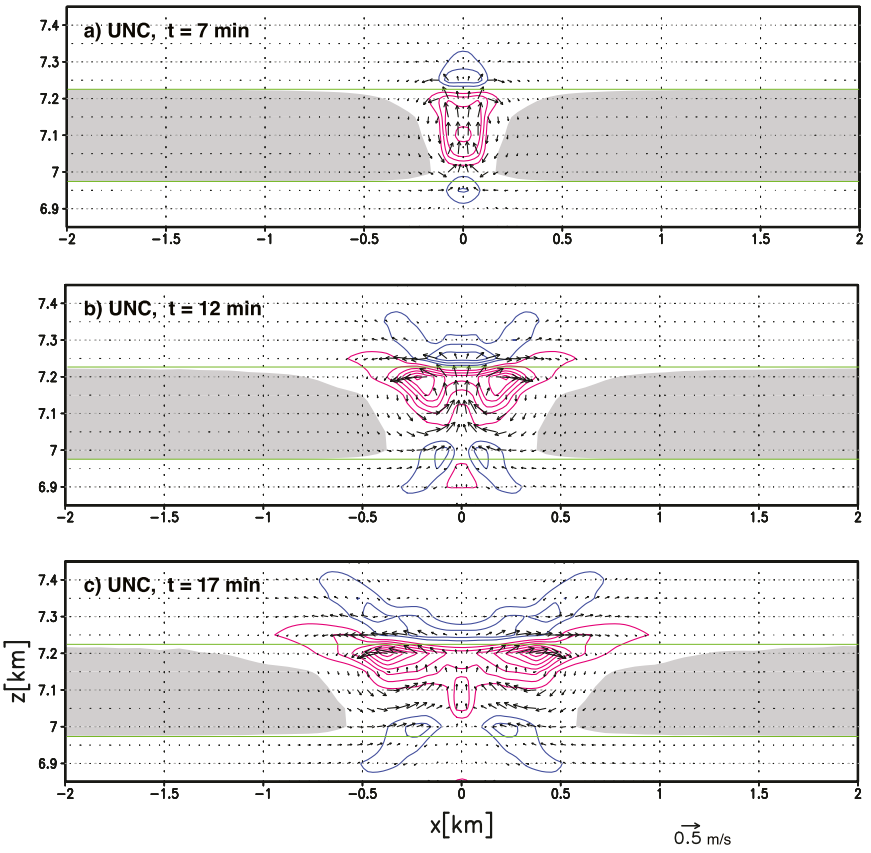

FIG. 5. Simulation of a holepunch in a uniform and marginal cloud layer (UNC). Shown are the same fields as in Fig. 3 with temperature anomaly contours at an interval of 0.05 K, and velocity arrows scaled on 0.5 m s^{-1}. Light shading indicates regions of liquid water mixing ratio q_l above 0.72×10^{-2} g kg^{-1} (smaller than CTL). The times chosen reflect development stages that roughly parallel those shown in Fig. 3.

criterion for distinguishing the regions of saturated and unsaturated air. In our model, we reference displacements from the lifting condensation level—the displacement $\tilde{\delta}_{\rm cl}$ for a parcel to achieve saturated conditions with exactly zero cloud water (Bohren and Albrecht 1998). At any point **x** within a moist fluid then, saturated conditions exist whenever the vertical displacement $\tilde{\delta}(\mathbf{x}, t)$ is above its condensation level

$$\tilde{\delta}(\mathbf{x},t) - \tilde{\delta}_{\rm cl}(\mathbf{x},t) > 0, \qquad (1)$$

as was a suggestion in Ogura and Phillips (1962). Finally, we consider the theory for a marginal cloud—those for which small displacements can evaporate the cloud so that linearized wave motions are sufficient to produce significant coupling to moisture. A similar linear coupling was applied in Bretherton (1987) for conditionally unstable convective clouds. This work adapts these ideas to a moist neutral situation more typical of stratiform cloud and includes forcing effects from weak latent heating by conversions of liquid and vapor to ice. The UNC simulation of Fig. 5 is an example of the dynamics for such a marginal cloud.

a. Equations for gravity wave motions

Our two-dimensional fluid model for the cloud dynamics is based upon the four familiar variables of gravity wave dynamics: vorticity $\tilde{\eta}(x, z, t)$, streamfunction $\tilde{\psi}(x, z, t)$, displacement $\tilde{\delta}(x, z, t)$, and buoyancy $\tilde{b}(x, z, t)$ (Sutherland 2010). The linear vorticity and displacement equations are

$$\frac{\partial \tilde{\eta}}{\partial t} = -\frac{\partial \tilde{b}}{\partial x} \quad \text{and}$$
$$\frac{\partial \tilde{\delta}}{\partial t} = -\frac{\partial \tilde{\psi}}{\partial x} = \tilde{w}, \qquad (2)$$

where the velocity relation $(\tilde{u}, \tilde{w}) = (\partial\tilde{\psi}/\partial z, -\partial\tilde{\psi}/\partial x)$ satisfies divergence-free flow and, by the definition of $\tilde{\eta}$, implies the streamfunction inversion

$$\frac{\partial^2\tilde{\psi}}{\partial x^2}+\frac{\partial^2\tilde{\psi}}{\partial z^2}=\tilde{\eta}. \tag{3}$$

For an isolated holepunch event in an otherwise quiescent fluid, the boundary conditions for this inversion will be periodic in x and $\tilde{\psi}=0$ at bounding z levels above and below—all sufficiently remote to minimize spurious wave effects. It then remains to present the fourth and remaining equation for $\tilde{b}(x, z, t)$ that embodies the buoyancy responses for dry, moist saturated, and moist unsaturated air.

b. Background profiles for dry and moist air

The vertical profile for the fluid is a dry and stratified tropospheric domain $-H<z<+H$ with a shallow layer of moist air centered at $z=0$. This layer, of thickness $D \ll H$, is designed to be moist neutral, and in addition, assumed very close to the exactly saturated conditions with zero liquid cloud. The moist fluid will therefore be everywhere near the tipping point where there is an asymmetry in the response to small vertical displacements. Upward displacement above the condensation point ($\tilde{\delta}-\tilde{\delta}_{\rm cl}>0$) will cause a switch of the buoyancy to that of moist neutral cloudy air. On the other hand, downward displacement below the condensation point ($\tilde{\delta}-\tilde{\delta}_{\rm cl}<0$) will lead to desaturation and a switch of the buoyancy to that of moist (stably) stratified clear air. The differences in the stratification for each of the fluid types are characterized by their (constant) Brunt–Väisälä frequencies

$$\tilde{N}^2(x,z,t) = \begin{cases} N_d^2, & \text{dry},\\ N_u^2, & \text{unsaturated and moist stably stratified},\\ 0, & \text{saturated and moist neutral}, \end{cases} \tag{4}$$

where the moist stratification is less than the dry, $N_u<N_d$. The criterion for saturation for moist air is Eq. (1), and $\tilde{\delta}_{\rm cl}$ does not apply for dry air. The buoyancy equation then takes the form

$$\tilde{b}(x,z,t)=\begin{cases} -\tilde{N}^2\tilde{\delta}, & \text{dry},\\ -\tilde{N}^2(\tilde{\delta}-\tilde{\delta}_{\rm cl})+\tilde{f}(x,z,t), & \text{moist} \end{cases} \tag{5}$$

that is continuous at the moist switch value ($\tilde{\delta}-\tilde{\delta}_{\rm cl}=0$). The prescribed forcing $\tilde{f}(x, z, t)$ is designed in section 3d to represent latent heating from ice processes within the moist region. Last, the assumption that the region of moist fluid is confined to the fixed layer $-D<z<+D$ requires that vertical displacements are much smaller than the layer depth, $\tilde{\delta} \ll D$.

c. The dimensionless model

The dimensions of the independent variables (x, z, and t) are based on a horizontal scale L and the dry Brunt–Väisälä time scale $1/N_d$. The moist layer is now on the scaled interval $-d<z<+d$ with $d=D/L$ and resides within in a deep domain $-h<z<+h$ with $h=H/L \gg d$. The linear Eqs. (2) and (3) can be nondimensionalized by scaling with the condensation level δ_c of the initial cloud. The velocities (u, w) scale on $N_d\delta_c$, vorticity (η) on $N_d\delta_c/L$, and streamfunction ψ on $N_d\delta_c L$. Buoyancy b scales on $N_d^2\delta_c$ so that Eq. (4) introduces the stratification parameter ratio $\alpha=N_u/N_d<1$. Note the assumption of small amplitude dynamics, as in the weak cloud water case of Fig. 5, is supported by the displacement scale $\delta_c \approx 25$ m being much less than the layer depth scale $D \approx 125$ m. The tildes are dropped with dimensionless fields and the independent variables interpreted consistently within this dimensionless context.

The dimensionless model consists of the four Eqs. (2), (3), and (5) with the tildes now removed. The scaled Brunt–Väisälä constants are

$$N^2(x,z,t) = \begin{cases} 1, & \text{dry},\\ \alpha^2, & \text{unsaturated and moist stably stratified},\\ 0, & \text{saturated and moist neutral}, \end{cases} \tag{6}$$

where the criterion for saturation within the moist layer is

$$\delta(x,z,t) - \delta_{\rm cl}(x,z,t) \begin{cases} >0, & \text{saturated cloudy air},\\ =0, & \text{saturated, zero liquid water},\\ <0, & \text{unsaturated clear air}. \end{cases} \tag{7}$$

d. Initiation of the holepunch

Without the explicit modeling of ice, the WBF initialization process cannot be represented directly within this fluid mechanical framework. Nonetheless, in this section we design an initial condensation level $\delta_{\rm cl}(x)$ and a latent heating term $f(x, z, t)$ in Eq. (5) that will yield faithful reproductions of the holepunch dynamics as produced in the full-physics simulations of section 2.

The microphysical response to the introduction of ice particles has two phases. It starts with the rapid depletion of cloud liquid (with its net release of latent heat of fusion) by the WBF process and follows with the deposition of vapor to ice (with its release of latent heat of sublimation). The simulations of section 2 confirm this two-stage sequence: the WBF liquid-to-ice conversion completes within the first 2 min, while much of the vapor-to-ice conversion occurs over the next 4 min. With our fluid model, we address the liquid conversion by the initial condition and the vapor conversion by the prescribed time-dependent buoyancy forcing [Eq. (5)].

The hole created in the moist layer by the WBF depletion of liquid has zero cloud water and leaves vapor at saturated with respect to liquid—this exactly corresponds to a zero condensation level $\delta_{\rm cl} = 0$. We describe the initial layer by a condensation level [Eq. (8)] with the time-independent form

$$\delta_{\rm cl}(x,z) = \begin{cases} 0, & \text{in } -1 < x < +1, \\ [-1 + e^{(1-x^2)/2x_0^2}]\cos(\pi z/2d), & \text{otherwise}, \end{cases} \tag{8}$$

that has a hole over the interval $-1 < x < +1$. The sinusoidal structure in the vertical gives a smooth tapering of the cloud to zero liquid at the top and bottom of the moist layer ($z = \pm d$) and maximum cloudiness at midlevel ($z = 0$). The Gaussian in x defines a localized disturbance that is continuous at the hole edges. The variance parameter x_0 controls the steepness of the edges and is used to adjust the relative width of the updraft. The latent heat of fusion associated with the creation of this initial hole is neglected relative to the much larger latent heating because of the vapor deposition that follows.

The vapor-to-ice conversion is modeled simply by a burst of positive buoyancy that decays in time—as occurs in the CTL simulation of Fig. 3. This buoyancy effect corresponds to an initial latent heating by deposition, followed by a later decay from the decrease in the available water vapor. For simplicity, we design this initial burst to have the same variations in spatial structure as in Eq. (8):

$$f(x,z,t) = \Delta b e^{-(t/t_0)^2/2} e^{-x^2/2x_0^2} \cos(\pi z/2d). \tag{9}$$

The Gaussian time dependence has its most rapid decay within $t < t_0$, so that subsequent wave motion is unforced propagation. Note that the raising of the condensation level associated with the loss of vapor in this process is neglected, as its impact on the dynamics via the buoyancy response [Eq. (5)] is estimated to be much less significant than this latent heating.

e. Gravity wave front

The numerical solutions to the nondimensionalized equations of section 3a [Eq.s. (2), (3), and (5)] are found using the method described in Muraki and Rotunno (2013, their section 3), but in this application all physical-diffusion and time-filter coefficients are set to zero. The dimensionless domain for the numerical solution is $-40 \le x \le +40$, $-40 \le z \le +40$, which is large enough to keep waves at the boundaries from affecting the domain center over the time of interest. The grid intervals are $dx = 80/720 \simeq 0.11$ and $dz = 80/360 \simeq 0.22$ and the time step for the leapfrog scheme is $dt = 0.01$.

Figure 6 shows the buoyancy anomaly and velocity vectors for a model solution designed to resemble the UNC simulation (Fig. 5). The stratification ratio in Eq. (6) is $\alpha^2 = (N_u/N_d)^2 = 1/5$. The holepunch configuration as defined by the initial condensation level [Eq. (8)] uses $d = D/L = 1$ and $x_0 = 1/2$. Last, the deposition heating as modeled in Eq. (9) uses $\Delta b = 1$, with a completion time scale for ice processes of $t_0 = 4.5$. This forcing strength is calibrated on a matching of the maximum potential temperature anomaly ($\Delta\theta_{\rm WRF} \approx 0.25$, around $t = 4$) realized in the updraft core of the UNC run. The dimensionless Δb is approximately

$$\Delta b = \frac{g}{N_d^2 \delta_c} \frac{\Delta\theta_{\rm WRF}}{\theta} \approx 1 \tag{10}$$

as obtained using the values stated in section 2, and is the only parameter that was not estimated through basic microphysical arguments.

Despite the simplified representations [Eqs. (8) and (9)] for the WBF microphysics, Fig. 6 shows a holepunch dynamics that reflects well the key features of the UNC simulated sequence. The earliest time[1] displayed ($t = 5$) has upward motion associated with a central buoyancy maximum whose compensating subsidence on either side has produced secondary buoyancy maxima and has begun to grow the hole. Because there is no moisture lost to (fallstreak) precipitation in the fluid model, the upward motion results in resaturation and the reappearance of cloud at

[1] Each unit of nondimensional time is approximately equal to 1 min of WRF simulation, since the time scale $N_d^{-1} \simeq 57$ s.

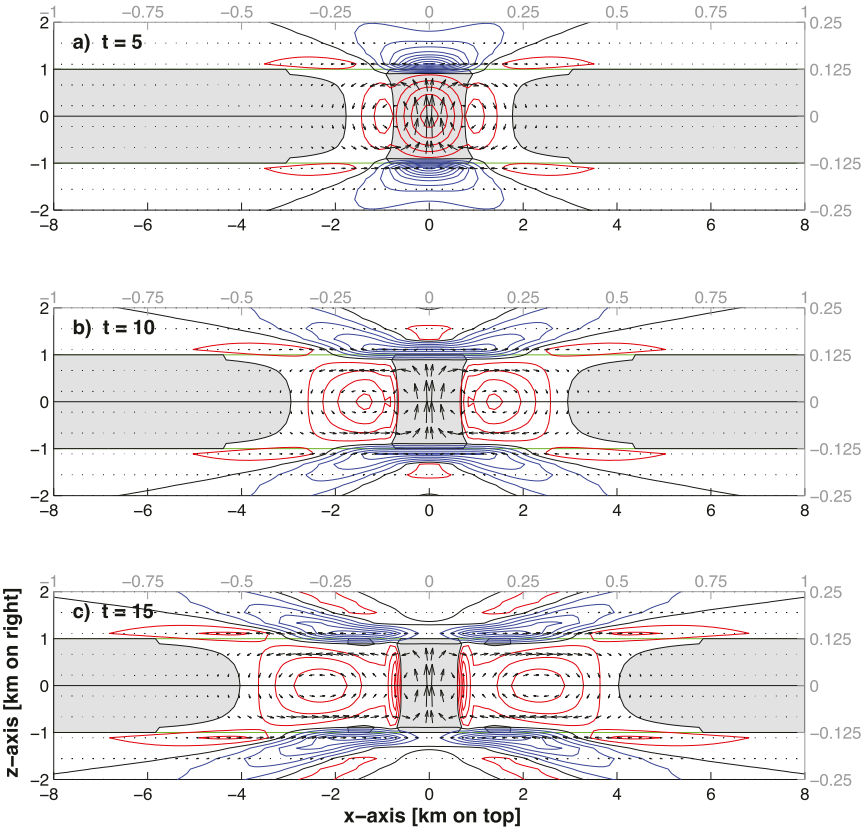

FIG. 6. Holepunch growth in the two-dimensional fluid model simulation. The gray shading indicates the saturated air within the moist layer (between the green levels). Buoyancy anomalies are contoured (interval = 0.1) with colors indicating positive (red), zero (black), and negative (blue). Flow arrows for velocity are scaled identically for all times, with $v_{max} = 1.77, 1.92,$ and 1.44 at $t =$ (a) 5, (b) 10, and (c) 15. The outward-propagating warm anomalies follow the cloud edge.

the core. Nevertheless, Fig. 6b at $t = 10$ shows that the lateral buoyancy maxima have strengthened, and the hole in the cloud layer has continued to widen. Figure 6c shows that by $t = 15$ each warm anomaly has produced an outward-propagating part and a nearly stationary inner part. The inner warming is due to subsidence driven by upward motion that is unchecked by adiabatic cooling within the moist neutral air of the resaturated core. Most importantly, however, the motion of the outward-propagating anomalies is largely independent of these inner-core details. These warm spots have fronts of subsidence on their outer edges, clearing more cloud and warming air at increasing distance from the center. Thus, the simple fluid model replicates well the key features of the WRF simulations: the expansion of the hole by an outward-propagating front of downward motion, as well as the radiation of gravity waves into the dry expanses. Moreover, the rate of spread is $\Delta x \simeq 1$ in $\Delta t = 5$, or in dimensional terms, 125 m/300 s = 0.42 m s^{-1} that is only slightly slower than the UNC simulation of Fig. 5.

4. A theory for the velocity of the cloud edge

Simulation using the fluid model of section 3 suggests that the expansion of the holepunch occurs by an outgoing gravity wave—propagating warm anomalies whose leading-edge front of downward motion clears the cloud. A similar gravity wave structure associated with a moving cloud-edge boundary arose in Muraki and Rotunno (2013) within the context of moist neutral, saturated airflow past a topographic ridge. In that situation, the appearance of clear air by sinking motion in the lee of the ridge generated both upstream- and downstream-propagating gravity waves. Specifically, the upstream-propagating feature was a front of subsidence which desaturated the incoming airstream. The influence of the moist neutral cloud was in determining the velocity of the (upstream) disturbance. It

was slower than the natural gravity wave speed and was determined by jump conditions local to the front. We demonstrate here that, within the buoyancy model of the previous section, the outward propagation of the holepunch cloud edge is similarly controlled.

a. *Rankine–Hugoniot formulas for the cloud-edge velocity*

Within the fluid mechanical model described in section 3c, the key mathematical property that allows the identification of front motion is that the dimensionless equations for vorticity and displacement [Eq. (2)] have the form of conservation laws (Lax 1973)

$$\frac{\partial \eta}{\partial t} + \frac{\partial b}{\partial x} = 0 \quad \text{and}$$
$$\frac{\partial \delta}{\partial t} + \frac{\partial \psi}{\partial x} = 0. \tag{11}$$

For any level z in the moist layer, cloud edges are moving points $x_e(t)$ where parcels are at their lifting condensation level, $\delta(x_e, z, t) - \delta_{\rm cl}(x_e, z, t) = 0$ [Eq. (7)]. At these points, there is a jump in stratification [Eq. (6)] across cloud edges that implies a discontinuous buoyancy derivative $\partial b/\partial x$ [Eq. (5)] despite the displacement being a continuous field. However, it is a property of any conservation law that a discontinuity in its solution must propagate at a speed satisfying a Rankine–Hugoniot (R–H) condition (Ockendon 2003). For the first equation of Eq. (11), the R–H condition involving the cloud-edge speed $x_e'(t)$ is

$$x_e'(t)\left[\frac{\partial \eta}{\partial x}\right]_-^+ + \left[\frac{\partial b}{\partial x}\right]_-^+ = 0, \tag{12}$$

where the square brackets denote differencing across the front discontinuities at $x_e(t)$. The derivation (not included here) is a standard argument applied to the x derivative of the vorticity equation [Eq. (11)] following the expectation that $\partial b/\partial x$ is discontinuous.[2] Here, we will use confirmation of this R–H speed condition [Eq. (12)] as a demonstration that the cloud edge is a propagating front.

Previous analysis of conservation laws in Muraki and Rotunno (2013) was simplified by the additional mathematical property that the system of equations was also hyperbolic. This permitted the use of the method of characteristics and the theory of shocks (Lax 1973). Here, however, the streamfunction inversion [Eq. (3)], by virtue of its elliptic PDE nature, breaks this hyperbolic property. It is usually the case that this loss of hyperbolicity also leads to the nonexistence (by smoothing or dispersion) of propagating discontinuities; but with discontinuous behavior built into the buoyancy equation [Eq. (5)] via the stratification [Eq. (6)], the cloud-edge fronts within our fluid model are a novel case of a free boundary (Ockendon 2003).

The computational confirmation of the R–H condition [Eq. (12)] raises two challenges: achieving sufficient numerical accuracy at the discontinuities and capturing the two-dimensional front structure. As a first approximation, we choose to bypass these complications by a reduction of our fluid model to a thin-layer analog that generates a one-dimensional front structure.

b. *An immersed layer approach*

The approximation strategy represents the moist region by a thin layer whose properties derive only from the values at level $z = 0$, yet still induces buoyancy effects throughout an $O(d)$ thick layer at the cloud height. This formulation borrows the basic idea behind the immersed boundary method that is used for computing the interaction of thin membranes with a fluid flow (Mittal and Iaccarino 2005). In this holepunch application, however, the moist layer is not itself in motion but has a property (specifically, buoyancy response) that evolves along the layer and couples with the external dry fluid. It is first demonstrated that the dynamics of this immersed layer (IL) approximation agrees well with the 2D fluid model and captures the motion of the cloud edge by a propagating wave front. The true frontal nature is then established by confirmation of the Rankine–Hugoniot speed [Eq. (12)].

The dimensionless vorticity equation is rewritten to decompose the buoyancy into the dry and moist contributions

$$\frac{\partial \eta}{\partial t} = -\frac{\partial b}{\partial x}[1 - S(z)] - \frac{\partial b}{\partial x}S(z), \tag{13}$$

where the function $S(z)$ indicates support limited to the moist region

$$S(z) = \begin{cases} 1, & \text{moist}(-d < z < +d), \\ 0, & \text{dry}. \end{cases} \tag{14}$$

Since the first right-hand-side term in Eq. (13) applies only in the dry fluid, substitution of the dimensionless dry buoyancy expression [$\partial b/\partial x = -\partial \delta/\partial x$; Eq. (5)] gives

[2] Another R–H condition can be derived from the second conservation law of Eq. (11) but involves discontinuities in $\partial^3\psi/\partial x^3$ and $\partial^3\delta/\partial x^3$ that are less amenable to accurate computing.

$$\frac{\partial \eta}{\partial t} = \frac{\partial \delta}{\partial x} - \left(\frac{\partial \delta}{\partial x} + \frac{\partial b}{\partial x}\right) S(z), \tag{15}$$

where the equation remains exact. The IL approach then involves two approximations beginning by an evaluation of the second term on the right side only using solution values at $z = 0$. Hence,

$$\frac{\partial \eta}{\partial t} \approx \frac{\partial \delta}{\partial x} - \left[\frac{\partial \delta(x,0,t)}{\partial x} + \frac{\partial b(x,0,t)}{\partial x}\right] \cos(\pi z/2d) S(z), \tag{16}$$

where the cosine profile is introduced for consistency with Eqs. (8) and (9). Then, the support function [Eq. (14)] is replaced with the smoother Gaussian profile

$$\cos(\pi z/2d) S(z) \rightarrow S_g(z) = e^{-z^2/2\sigma^2}. \tag{17}$$

The width parameter, $\sigma^2 = (8/\pi^3)d^2$, normalizes the area integral to be the same under both profiles, and $S_g(0) = 1$ ensures that the $\partial\eta/\partial t$ at $z = 0$ only depends on the moist buoyancy [Eq. (5)]. The equations for dimensionless displacement [Eq. (2)] and streamfunction [Eq. (3)] are now completed with the IL vorticity equation

$$\frac{\partial \eta}{\partial t} - \frac{\partial \delta}{\partial x} = \left[\frac{\partial \delta(x,0,t)}{\partial x} + \frac{\partial b(x,0,t)}{\partial x}\right] S_g(z), \tag{18}$$

for which the moist layer is no longer a distinct region, but acts as an immersed forcing within a dry, stratified fluid. At $z = 0$, the moist buoyancy [Eq. (5)] includes both the heating and the moisture switch

$$b(x,0,t) = f(x,0,t) + \begin{cases} -\alpha^2[\delta(x,0,t) - \delta_{\rm cl}(x,0)], & \text{unsaturated}, \\ 0, & \text{saturated}, \end{cases} \tag{19}$$

with the saturation criterion $\delta(x, 0, t) - \delta_{\rm cl}(x, 0) > 0$. All fields are initially zero, and the holepunch dynamics are initiated through the forcing $f(x, 0, t)$ in Eq. (19).

c. The IL holepunch computation

Despite that the solutions to the IL have discontinuities at cloud edges, a spectral solver can be used to compute an accurate front velocity. The solution variables best computed are streamfunction $\psi(x, z, t)$ and displacement $\delta(x, z, t)$ since they remain continuous through two x derivatives. A key advantage of the IL simplification, where the moist switch [Eq. (5)] is only applied at the cloud level $z = 0$, is that buoyancy discontinuities can only arise from the moist values $b(x, 0, t)$. Since these discontinuities are communicated to the rest of the domain through

$$b(x,z,t) = \delta(x,z,t) - [\delta(x,0,t) + b(x,0,t)] S_g(z) \tag{20}$$

the fronts are not curved (as seen in Fig. 6). This implies that solutions are smooth to all orders of the z derivative and lends additional robustness to the spectral computation. For spectral accuracy, the discontinuous buoyancy derivative [Eq. (18)] is calculated with the switch [Eq. (19)] applied after pseudospectral differentiation.

d. The IL holepunch dynamics

Buoyancy and flow velocity from computing the IL approximation are shown as Fig. 7 for $t = 5$, 10, and 15. The physical parameters used are identical to those of the 2D simulation of Fig. 6. The spectral collocation gives a resolution of 1/512 in both x and z directions, with adaptive time stepping. Intervals of saturated moist buoyancy (cloud) are indicated by a thick dark line along $z = 0$. Although a moist-layer depth is only implicitly introduced as the variance width of the Gaussian in Eq. (17), the green lines at $z = \pm d$ give a clear visual impression of an induced moist-layer structure. At $t = 5$, the dominant feature is the central updraft with outlying descent that is clearing the cloud edge. By $t = 10$, the splitting of warm anomalies from the center of the hole has occurred. At $t = 15$, the flow circulation has clearly organized around the two warm anomalies, and the formation of the propagating wave front is complete. The pattern of the weak radiation away from the moist layer compares well with the 2D fluid model, as does the appearance of the resaturated air at the holepunch core.

Figure 8 demonstrates that the outer cloud edge is moving as a frontal discontinuity in the IL model. The speed $x_e'(t)$ is obtained by two distinct methods: the black circles are obtained from the time derivative of the cloud-edge condition [Eq. (7)], and the red line is determined by the R–H jump condition [Eq. (12)]. The location of the front $x_e(t)$ is estimated by linear interpolation for the zero crossing of the condensation level condition [Eq. (7)]. However, a more accurate speed (black circles) is obtained from the total t derivative of the zero cloud water condition [Eq. (7)] at $x = x_e(t)$ and $z = 0$:

$$\frac{d}{dt}\{\delta[x_e(t),0,t] - \delta_{\rm cl}[x_e(t),0]\} = x_e'(t)\left(\frac{\partial \delta}{\partial x} - \frac{\partial \delta_{\rm cl}}{\partial x}\right) - \left(\frac{\partial \psi}{\partial x}\right) = 0. \tag{21}$$

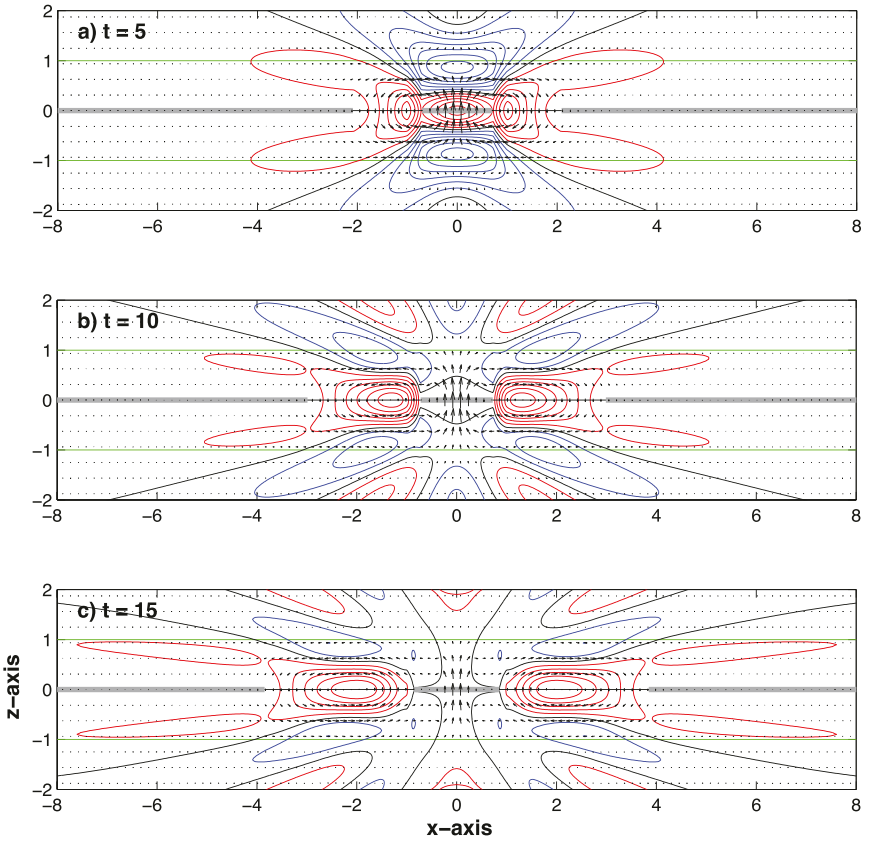

FIG. 7. Holepunch growth in the immersed layer model simulation. Thick dark lines along the idealized moist layer at $z = 0$ indicate regions of cloudlike saturated buoyancy response. Buoyancy anomalies are contoured as in Fig. 6. Arrows for flow velocity are scaled identically for all times, with $v_{max} = 2.20, 2.13,$ and 1.57 at $t =$ (a) 5, (b) 10, and (c) 15.

The final form above involves substitution of the time derivative with Eq. (11), and the accuracy comes from the pseudospectral evaluation of the spatial derivatives. For the speed (red line) from the R–H equation [Eq. (12)], the derivative jumps are estimated by three-point polynomial extrapolation. The speed comparison is shown only for times after $t = 4$ as the extrapolations are not reliable until the clear-air region spans a sufficient number of grid points. At $t = 15$, the IL front is propagating at a (dimensional) speed close to 0.4 m s^{-1}, which

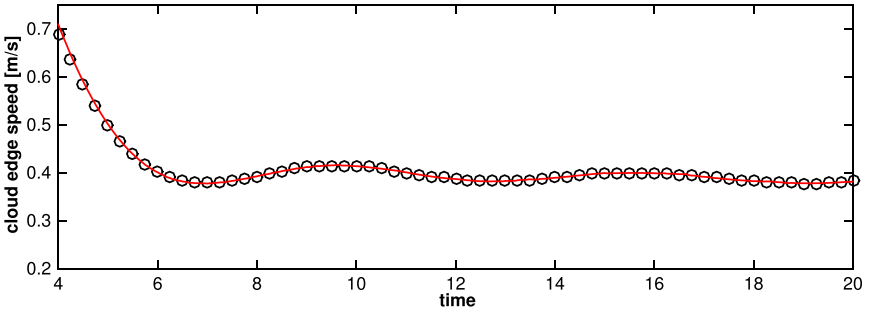

FIG. 8. Comparison of the dimensional cloud-edge speed for the immersed layer model (for the rightmost edge in Fig. 6). The red line is the speed as computed using the Rankine–Hugoniot jump condition [Eq. (12)]. Black circles confirm consistency with the motion [Eq. (21)] of the cloud-edge position, $x_e(t)$—thus establishing the frontal nature of the holepunch expansion.

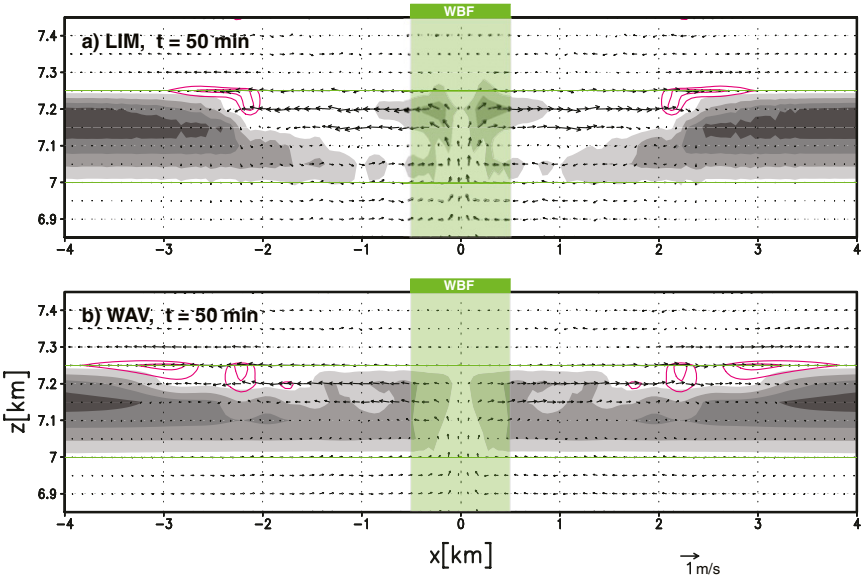

FIG. 9. WRF comparison of holepunch dynamics for an adiabatic cloud layer after 50 min. Fields as shown in Fig. 4a, but only the warmest contours (red, 0.2 and 0.3 K) are indicated and liquid water mixing ratio $q_l = 1, 3, 5, 7 \times 10^{-2}$ g kg^{-1} are highlighted that detail the vanishing cloud. The LIM run is a continuation from Fig. 4a. (a) The moist neutral cloud in LIM is contrasted against (b) WAV for which the latent heat from (non-WBF) evaporation is suppressed, so that cloudy air responds as a (weakly) moist stratified fluid. The hole is more effectively opened when the cloudy air is moist neutral, as the resulting coherent front of subsidence (LIM) produces a greater amount of permanent downward displacement than a laterally dispersing wave train (WAV).

compares very well with the two-dimensional fluid model. The slight oscillations in the front speed are attributed to waves propagating within the clear-air layer. The upshot of this 1D analysis is that the cloud edge propagates as a frontal discontinuity, and its propagation speed is determined by local jump conditions.

5. In closing

The analysis presented here determines that, in the case of a marginal cloud, linear wave theory identifies a gravity wave front of subsidence as the mechanism for the sustained expansion of a holepunch cloud. However, the full-physics WRF simulations show that the holepunch is possible over a range of cloud profiles encompassing small-displacement (UNC) to finite-displacement (ADC) dynamics. To illustrate the importance of the frontal nature of the disturbance to the opening of the holepunch even in the case of an adiabatic cloud, we contrast with a final WRF run in which the front cannot form. The WAV run is identical to the LIM run except that the latent heating of non-WBF cloud evaporation is suppressed (Fig. 9), so the entire WAV moist layer acts as a uniform, weakly stratified fluid for both clear and cloudy air. As a result, the WAV run produces the expected wave train of outward-propagating warm cells (Fig. 9b). The outcome of this difference is apparent in the detailed cloud structure where the coherent front of subsidence (LIM) produces more clearing by permanent downward displacement than a laterally dispersing wave train (WAV). This supports the idea that the frontal mechanism identified within the specialized marginal cloud case is a general dynamical feature of the holepunch.

In this study, an alternative explanation for the continued growth of the holepunch by a gravity wave front is presented. The mechanism identified here is different from existing hypotheses that rely upon continuous ice processes and is encapsulated in the cartoon in Fig. 10. The initial ice injection creates a localized updraft, but the outward propagation of the warm anomalies proceeds without the requirement of direct forcing by further WBF processes. An important consequence of the slowing of the front is a persistent subsidence that enhances the clearing of the cloud.

Acknowledgments. Support for DJM provided by NSERC RGPIN-238928. DJM also thanks the MMM Division of NCAR for their intellectual hospitality during the course of this work.

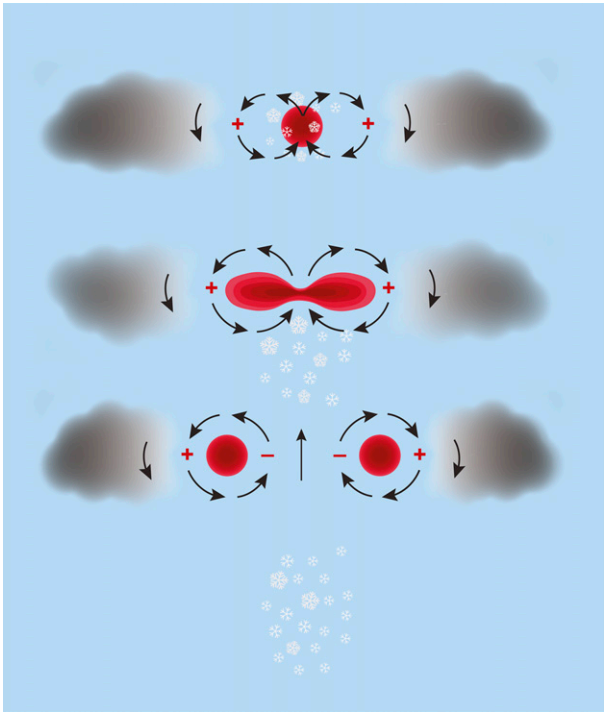

FIG. 10. Cartoon for the evolution of the gravity wave front. (top) A localized warm anomaly generates a central updraft where the outlying subsidence desaturates the moist air. (middle) Continued sinking on the leading edge spreads the warm anomaly, and in this manner initiates the outward propagation of a pair of warm buoyancy anomalies—all the while enlarging the hole. (bottom) As gravity waves cannot propagate within moist neutral air, the cloud edge moves outward as a wave front. Snowflakes illustrate fallstreak regions of falling ice crystals.

APPENDIX

WRF Model Description and Experimental Design

This study employs the Weather Research and Forecasting (WRF) Model, version 3.5.1 (Skamarock et al. 2008). WRF is a nonhydrostatic, compressible atmospheric model. The governing equations are solved using a time-split integration with third-order Runge–Kutta scheme. Horizontal and vertical advection are calculated using fifth- and third-order discretization schemes, respectively, with modifications to ensure monotonicity (Wang et al. 2009). The model setup is two dimensional with periodic lateral boundaries and a domain 30 km wide and 20 km deep. The upper boundary is a rigid lid with a Rayleigh damper and damping coefficient of $0.003\,s^{-1}$ applied to the top 5 km. The horizontal grid spacing is 50 m and vertical grid spacing approximately 50 m, with a slight stretching from model bottom to top. Diffusion is implicit through the use of odd-order advection schemes. The model time step is 1 s, with substepping applied for acoustic modes. Microphysical processes are treated using the two-moment bulk scheme of Morrison et al. (2005, 2009). Other physical processes such as radiation are neglected for simplicity.

A set of simulations with differing initial conditions was performed to explore the behavior of the holepunch dynamics simulated by WRF—an overview is given in Table A1. These experiments were only slightly modified from those used for the simulations of Heymsfield et al. (2011), and the initial thermodynamic profiles used are shown in Fig. 2. The difference in the cloud layers is an initialization that imposes moist neutrality in a manner consistent with the WRF thermodynamics [Heymsfield et al. (2011) assumed only quasi–moist neutral conditions]. The condition for a zero Brunt–Väisälä frequency (Emanuel 1994), along with the WRF equations for the first law of thermodynamics and hydrostatic balance, were discretized and integrated upward from cloud base [Miglietta and Rotunno (2005), see their section 2]. At each vertical level of the discretized equations, the moist thermodynamics and hydrostatic equations were solved by iteration to produce consistent values of potential temperature, saturation vapor pressure, and air density—ensuring initial N_m^2 that were smaller than $1\times10^{-6}\,s^{-2}$. In the vertical integration for the adiabatic moist layers (CTL, ADC), the total water mixing ratio $\overline{q}_T$ was set at a constant value with height. For the uniform moist layer (UNC), the liquid cloud water mixing ratio was taken to be constant, $\overline{q}_l = 0.015\,g\,kg^{-1}$, a value that also reduced the total cloud water to one-quarter of ADC.

Ice initiation of the holepunch was done by injecting a concentration of ice crystals 10 s into the simulation over a region five grid points (250 m) wide throughout the depth of the cloud layer. The number mixing ratio of

TABLE A1. Summary of the WRF simulations.

Run	Figure No.	Description
CTL	Fig. 3	Control run with moist neutral and moist adiabatic cloud layer
LIM	Figs. 4a, 9a	As in CTL, except WBF process limited to within 250 m from the hole center (green shading)
ADC	Fig. 4b	As in CTL, but for modifications to the static stability and RH above and below the cloud layer
UNC	Fig. 5	As in ADC, but for 1) uniform cloud water mixing ratio and 2) reduction by one-quarter of total cloud water and concentration of injected ice crystals
WAV	Fig. 9b	As in LIM, but for latent heating from non-WBF evaporation turned off (moist stratified cloud)

injected particles was $500\,\mathrm{kg}^{-1}$ ($\approx 250\,\mathrm{L}^{-1}$), except for the marginal cloud case (UNC) where this was also reduced by one-quarter ($125\,\mathrm{kg}^{-1}$). Note that in all simulations the only conversion process from liquid water to ice is the WBF mechanism; riming is neglected for simplicity.

Although the initial WBF heating is lessened in the UNC case, since the cloud water content has also been reduced, a holepunch similar to CTL and ADC still occurs despite the reduced vertical motions. Assuming the total evaporation of the liquid occurs by downward parcel displacement (neglecting the moist entropy gradient), the displacement from the condensation level is approximated by the vertical increase of carrying capacity of vapor required to evaporate all of the liquid. This gives the approximate relation

$$\delta_c \frac{d\overline{q}_v}{dz} \approx \overline{q}_l, \tag{A1}$$

which implies a downward displacement for total evaporation as apparent from the (negative) gradient of the background vapor mixing ratio $\overline{q}_l$ in Fig. 2. Estimating the gradient $\Delta\overline{q}_l \approx 1.04\,\mathrm{g\,kg}^{-1} - 0.92\,\mathrm{g\,kg}^{-1}$ over 250 m, the liquid water mixing ratio $\overline{q}_l = 0.015\,\mathrm{g\,kg}^{-1}$ gives $\delta_c \approx 25$ m. This is considerably less than the 250-m total depth of the layer and connects the UNC simulation with the marginal cloud theory.

REFERENCES

Bjerknes, J., 1938: Saturated ascent of air through a dry-adiabatically descending environment. *Quart. J. Roy. Meteor. Soc.*, **64**, 325–330.

Bohren, C. F., and B. A. Albrecht, 1998: *Atmospheric Thermodynamics.* Oxford, 416 pp.

Bretherton, C. S., 1987: A theory for nonprecipitating moist convection between two parallel plates. Part I: Thermodynamics and "linear" solutions. *J. Atmos. Sci.*, **44**, 1809–1827, doi:10.1175/1520-0469(1987)044<1809:ATFNMC>2.0.CO;2.

Cushman-Roisin, B., 1994: *Introduction to Geophysical Fluid Dynamics.* Prentice-Hall, 320 pp.

Emanuel, K. A., 1994: *Atmospheric Convection.* Oxford University Press, 592 pp.

Heymsfield, A., 2013: Reply to "Comments on 'Aircraft-Induced Hole-Punch and Canal Clouds: Inadvertent Cloud Seeding.'" *Bull. Amer. Meteor. Soc.*, **94**, 1408–1409, doi:10.1175/BAMS-D-13-00038.1.

——, P. C. Kennedy, S. Massie, C. Schmitt, Z. Wang, S. Haimov, and A. Rangno, 2010: Aircraft-induced hole punch and canal clouds: Inadvertent cloud seeding. *Bull. Amer. Meteor. Soc.*, **91**, 753–766, doi:10.1175/2009BAMS2905.1.

——, G. Thompson, H. Morrison, A. Bansemer, R. M. Rasmussen, P. Minnis, Z. Wang, and D. Zhang, 2011: Formation and spread of aircraft-induced holes in clouds. *Science*, **333**, 77–81, doi:10.1126/science.1202851.

Hindman, E. W., 2013: Comments on "Aircraft-Induced Hole-Punch and Canal Clouds: Inadvertent Cloud Seeding." *Bull. Amer. Meteor. Soc.*, **94**, 1407–1407, doi:10.1175/BAMS-D-12-00088.1.

Hobbs, P. V., 1985: Holes in clouds. *Weatherwise*, **38**, 254–258, doi:10.1080/00431672.1985.9954914.

Johnson, H. M., and R. L. Holle, 1969: Observations and comments on two simultaneous cloud holes over Miami. *Bull. Amer. Meteor. Soc.*, **50**, 157–161.

Kuo, H. L., 1961: Convection in conditionally unstable atmosphere. *Tellus*, **13**, 441–459, doi:10.1111/j.2153-3490.1961.tb00107.x.

Lax, P. D., 1973: *Hyperbolic Systems of Conservation Laws and the Mathematical Theory of Shock Waves.* SIAM, 48 pp., doi:10.1137/1.9781611970562.

Ludlam, F. H., 1956: Fall-streak holes. *Weather*, **11**, 89–90, doi:10.1002/j.1477-8696.1956.tb00297.x.

Miglietta, M. M., and R. Rotunno, 2005: Simulations of moist nearly neutral flow over a ridge. *J. Atmos. Sci.*, **62**, 1410–1427, doi:10.1175/JAS3410.1.

Mittal, R., and G. Iaccarino, 2005: Immersed boundary methods. *Annu. Rev. Fluid Mech.*, **37**, 239–261, doi:10.1146/annurev.fluid.37.061903.175743.

Morrison, H., J. A. Curry, and V. I. Khvorostyanov, 2005: A new double-moment microphysics parameterization for application in cloud and climate models. Part I: Description. *J. Atmos. Sci.*, **62**, 1665–1677, doi:10.1175/JAS3446.1.

——, ——, and ——, 2009: Impact of cloud microphysics on the development of trailing stratiform precipitation in a simulated squall line: Comparison of one- and two-moment schemes. *Mon. Wea. Rev.*, **137**, 991–1007, doi:10.1175/2008MWR2556.1.

Muraki, D. J., and R. Rotunno, 2013: Internal gravity waves in a saturated moist neutral atmosphere. *J. Atmos. Sci.*, **70**, 3693–3709, doi:10.1175/JAS-D-13-051.1.

Ockendon, J. R., 2003: *Applied Partial Differential Equations.* Oxford University Press, 464 pp.

Ogura, Y., and N. A. Phillips, 1962: Scale analysis of deep and shallow convection in the atmosphere. *J. Atmos. Sci.*, **19**, 173–179, doi:10.1175/1520-0469(1962)019<0173:SAODAS>2.0.CO;2.

Pauluis, O., and J. Schumacher, 2010: Idealized moist Rayleigh-Benard convection with piecewise linear equation of state. *Commun. Math. Sci.*, **8**, 295–319, doi:10.4310/CMS.2010.v8.n1.a15.

——, and ——, 2011: Self-aggregation of clouds in conditionally unstable moist convection. *Proc. Natl. Acad. Sci. USA*, **108**, 12 623–12 628, doi:10.1073/pnas.1102339108.

Pedgley, D. E., 2008: Some thoughts on fallstreak holes. *Weather*, **63**, 356–360, doi:10.1002/wea.279.

Poulter, R. M., 1948: Man-made cirrus? *Weather*, **3**, 232–233, doi:10.1002/j.1477-8696.1948.tb00922.x.

Schumacher, V. C., 1940: Beobacktungen an einer altokumulusdecke. *Z. Angew. Meteor.*, **57**, 214.

Scorer, R. S., 1964: Fallstreak holes. *Weather*, **19**, 90–91.

Simon, A., 1966: Dissipation dun altocumulus sur le pasage dun avion a reaction. *J. Rech. Atmos.*, **2**, 36–38.

Skamarock, W. C., and Coauthors., 2008: A description of the Advanced Research WRF version 3. NCAR Tech. Note NCAR/TN-4751+STR, 113 pp., doi:10.5065/D68S4MVH.

Sutherland, B. R., 2010: *Internal Gravity Waves.* Cambridge University Press, 394 pp.

Wang, H., W. C. Skamarock, and G. Feingold, 2009: Evaluation of scalar advection schemes in the Advanced Research WRF model using large-eddy simulations of aerosol–cloud interactions. *Mon. Wea. Rev.*, **137**, 2547–2558, doi:10.1175/2009MWR2820.1.

Westbrook, C., and O. Davies, 2010: Observations of a glaciating hole-punch cloud. *Weather*, **65**, 176–180, doi:10.1002/wea.504.